


Prediction of Rock Compressive Strength Using Machine Learning Algorithms Based on Spectrum Analysis of Geological Hammer

Qiubing Ren · Gang Wang · Mingchao Li  · Shuai Han

Received: 31 March 2018 / Accepted: 6 July 2018 / Published online: 12 July 2018
© Springer Nature Switzerland AG 2018

Abstract The traditional method to estimate rock compressive strength (RCS) in field operation is dependent on hammering rocks and artificial identification. It is too subjective to get high estimation accuracy. For this reason, the new and non-destructive method uses machine learning algorithms to analyze acoustic characteristics of geological hammer to predict RCS accurately. The hammering sound samples were successively preprocessed by signal enhancement algorithm and double-threshold method to reduce noise and acquire valuable intervals of all. We have also performed the time-frequency domain conversion on sound signal through FFT, which obtained two brand new indexes, amplitude attenuation coefficient and high and low frequency ratio, as the input parameters of models. By contrasting the performance of various models based on k -nearest neighbors, naive Bayes, random forest, artificial neural networks (ANN), and support vector machines (SVM), we uncovered that the prediction accuracy of both SVM and ANN was over 95%, superior to others. Thus, SVM and ANN were better for widespread

application in geological surveys and construction acceptance to predict RCS accurately. In addition, characteristic mechanism of acoustic spectrum was explained from microstructure, energy dissipation and filter effect, which indicated why there existed strong correlation between acoustic characteristics and RCS. The current rock mass classification standard was supplemented with the above two characteristic indexes for better identification.

Keywords Rock compressive strength · Geological hammer · Spectrum analysis · Machine learning algorithms · Rock mass classification

1 Introduction

Rock compressive strength (RCS) is one of the most important and basic mechanical properties in rock mechanics and is also the main index that reflects a rock's failure to withstand external forces. Using the RCS value, the physical and mechanical properties of rocks can be measured, rock failure criteria can be established, and other rock mechanical parameters can be estimated. Thus, it has become important to develop a simple method that reliably measures RCS for use in construction, geology, water conservation, etc. Various methods of measuring RCS have been explored, including the empirical discriminant

Q. Ren · M. Li (✉) · S. Han
State Key Laboratory of Hydraulic Engineering
Simulation and Safety, Tianjin University,
Tianjin 300354, China
e-mail: lmc@tju.edu.cn

G. Wang
Chengdu Engineering Corporation Limited, PowerChina,
Chengdu 410014, China

method, rock statics determination method, indirect testing method and machine learning algorithms (MLAs) modeling prediction method.

The empirical discriminant method is a rule of thumb of RCS based on the strike note produced by hammering rocks and is dependent on the experience of the geologist and the specific conditions of the site. It is a commonly used method in domestic and international geological surveys and construction acceptance (BS5930 1981; Marinos and Hoek 2001; Hack and Huisman 2002). However, the method is subjective and influenced by many factors such as lack of experience and negligence, which reduce the accuracy of the estimated RCS value.

In the rock statics determination method, indoor and outdoor mechanical rock test (Hencher and Richards 2015) in accordance with testing methods provided by the International Society for Rock Mechanics and Rock Engineering (ISRM) (Ulusay 2014) are used to directly determine the external load of core specimen failure, which is used to mathematically determine strength value. Experimental test values are closer to the true value than the empirical discriminant method, but it is arduous and time-consuming due to the need of high-quality core specimens. Moreover, it is not practical for research projects because the instrument used for testing is not portable and the operation steps are tedious.

Indirect testing method establishes the relationship between rock mechanics and indirect parameters (Karakus and Tutmez 2006; Karaman and Kesimal 2015) such as Schmidt rebound value and ultrasonic velocity, which are affected by porosity and anisotropy, and can be used to calculate the RCS value of a rock. The method is effective for most qualities of rock specimens and the instruments used for testing are simple to operate, thus it is a convenient way to measure RCS value and suitable for testing in the field. However, taking the rebound test as an example, there are also some limitations of the approach, i.e., it is not suitable for rocks with poor surface properties.

With the rapid development of computer technique and artificial intelligence, artificial neural networks (ANN), support vector machines (SVM), and other algorithms have become more popular. In MLAs modeling prediction, these algorithms are applied to obtain valuable information from trial data. Once a universal statistical regression prediction model has been established, it can be used to predict the RCS

values of most rocks (Momeni et al. 2015; Mohamad et al. 2015). The advantages of this method include its strong adaptability, high accuracy, and the ability to construct a model once and refer to it multiple times. MLAs are often combined with other test methods to make up for its inability to account for the wide variety of rocks and huge differences of occurrence conditions.

In recent years, many achievements have been made by MLAs in pattern recognition, function approximation, and modeling simulation (Jordan and Mitchell 2015; Fattahi and Karimpouli 2016). MLAs have also been widely used in rock mechanics and engineering (Li et al. 2014; Fattahi 2017; Valera et al. 2018). Based on this, we proposed a new and non-destructive method combined by MLAs and indirect test to determine RCS according to the hammering sound. Our work used MLAs to study the correlation of acoustic characteristics of geological hammer and RCS value based on different circumstances regarding the sample. Time and frequency domain analysis were combined to analyze the hammering sound from the rock, and the correlation between acoustic characteristics and RCS was used to differentiate mechanical properties of different rocks. The RCS prediction models were established based on k -nearest neighbors (KNN), Naive Bayes (NB), random forest (RF), ANN, and SVM, which were then compared and evaluated for accuracy and performance. Finally, the model with the best performance was determined to be a reliable tool for RCS prediction. The novel research method combined with data science, acoustics, and rock mechanics eliminates experiential error caused by subjective factors and is simple to operate, thus enlarging the category of acoustic survey in engineering practice.

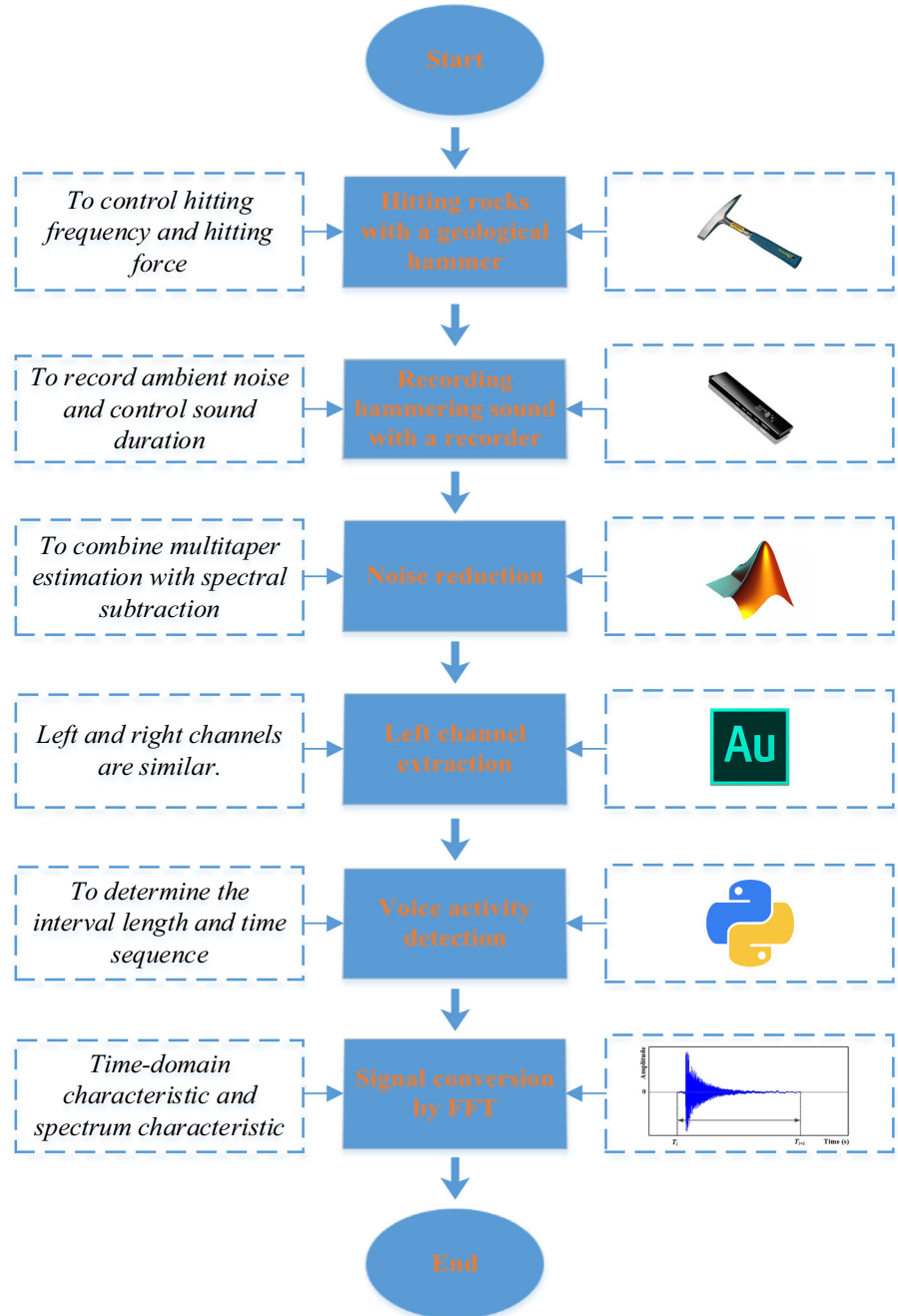
2 Signal Acquisition and Processing

The Newsmy V03 voice recorder was selected as the recording device, which featured dual-channel sampling at a frequency of 24 kHz. The measuring point of each rock was hit by a geological hammer at least 150 times in a row during a 3-min duration, ensuring that the interval between two hits was long enough to allow the sound of the first hit to decay to ambient noise. In order to account for the influence of ambient noise during field tests, ambient noise was recorded for

3 min before hammering at each rock and was later used for noise reduction. Additionally, all hammering tests were performed by a fixed person to minimize user error and the effect of the difference on the quality of the acoustic signal was eliminated so that the

acoustic waveform did not change significantly with hitting force. Figure 1 demonstrated the procedure of acoustic signal acquisition and preprocessing.

Fig. 1 Implementation procedure of signal acquisition and preprocessing



2.1 Signal Preprocessing

2.1.1 Signal Enhancement

The rock hammering sound recorded in field operation was non-stationary acoustic signal, containing a large amount of invalid sound influenced by external airflow and ambient noise, which cannot be directly used to extract characteristic parameters. Signal enhancement was adopted to restore real sound. There was a significant overlap between ambient noise and hammering sound. The traditional digital filters (IIR and FIR) were difficult to denoise effectively because hammering sound was short and powerful, while ambient noise was additive and stable. An enhanced signal enhancement algorithm based on short-term spectral estimation was used to eliminate noise. We combined multitaper estimation with spectral subtraction (Berouti et al. 1979; Thomson 1982) to apply to large range of SNR. The compositing method also had small computation amount and strong real-time performance. The result of noise reduction was shown in Fig. 2. The quality of signal was improved after signal enhancement, with SNR increased by 2.68 dB. The removal of ambient noise was obvious, and the signal waveform did not have a significant distortion. At the same time, the subjective audio-visual result also indicated that there was no significant difference from the original sound.

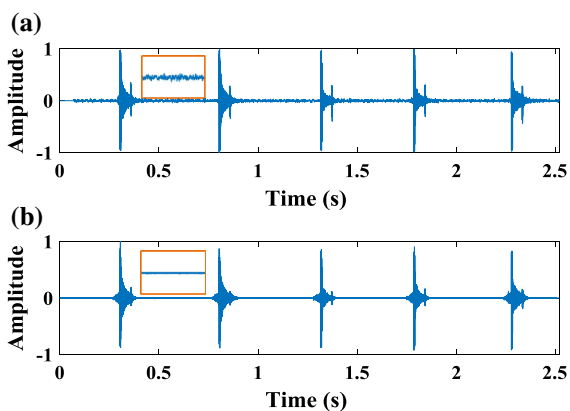


Fig. 2 Signal waveforms **a** before noise reduction and **b** after noise reduction

2.1.2 Voice Activity Detection

The audio data of geological hammer was split into the left and right channel for subsequent processing. Since the difference between the two-channel waveform was insignificant, the left channel waveform was chosen as the representative signal for the hammering sample. Voice activity detection (VAD) (Li et al. 2002) was a key link in signal analysis and recognition, which can find the starting point and endpoint from the audio file containing multiple acoustic signals for storing the effective signal. We chose double-threshold algorithm (Lee et al. 2003) which coupled short-term average energy (or energy for short) with zero-crossing rate (ZCR) to detect the endpoint of the hammering sound sample. The improved double-threshold algorithm was implemented by second-order decision mechanism. We set both the lower threshold T_1 and the higher threshold T_2 as dynamic values because of the ever-changing noise and the difference of hammering force. The two thresholds were respectively selected for preliminary judgment in terms of short-term average energy envelope after signal framing. The threshold T_3 was selected on the basis of ZCR as a further filter, which helped to extend the length of hammering sound to ensure the integrity of spectrum information of each effective signal. Thus, the endpoint of each effective signal was determined by comparing frame by frame. Figure 3 summarized the result of endpoint detection of hammering sound samples. It can be seen that double-threshold algorithm can detect the effective signal interval accurately. After endpoint detection, a total of 2014 independent and effective time-domain acoustic signal segments were acquired, as shown in Table 1.

Signal conversion was performed to extract acoustic characteristics of hammering sound. For more accurate and insightful analysis of spectrum, the time-domain signal was converted into the frequency-domain signal through FFT (Kido 2015). Thus, the complex signal was transformed into superimposed sinusoidal signals to analyze the amplitude, energy, and phase relationships of various frequency components contained in the frequency-domain signal, thereby analyzing spectrum characteristics of the signal. The above two signal analysis methods were complementary and integral. We combined both approaches organically to thoroughly analyze the

Fig. 3 Endpoint detection **a** result of VAD, **b** short-term average energy, and **c** ZCR frame by frame

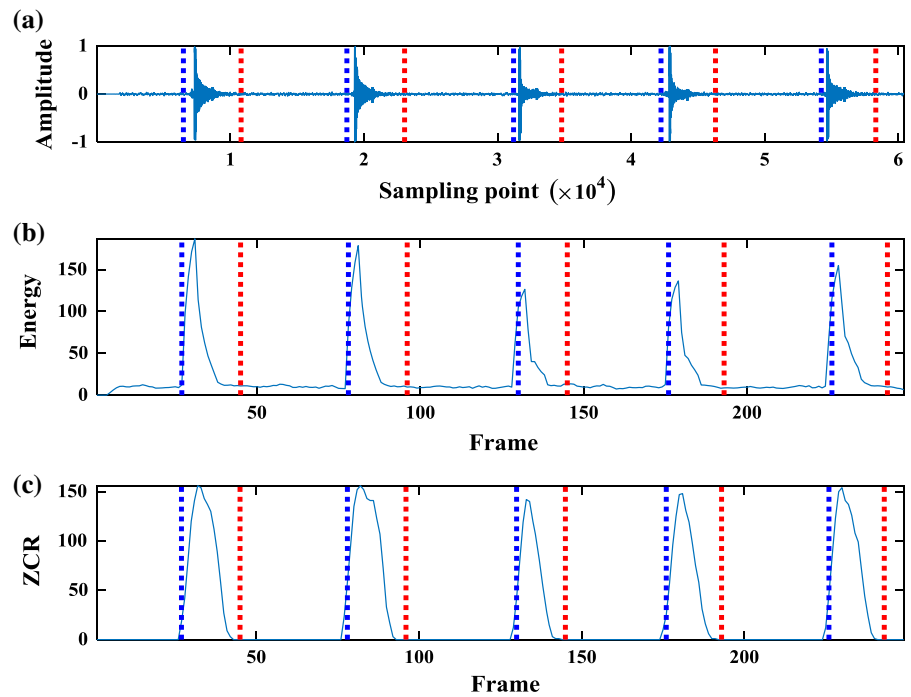


Table 1 Summary of signal acquisition, preprocessing and classification results

Rock specimen number	RCS	Number of effective signal intervals	Number of training set	Number of test set
1	71.20	223	179	44
2	64.20	164	131	33
3	73.00	232	186	46
4	48.33	246	197	49
5	38.47	239	192	47
6	61.87	230	184	46
7	54.00	204	164	40
8	67.33	231	185	46
9	58.33	245	196	49
Total		2014	1614	400

acoustic signal of geological hammer from different aspects (Boashash 2015).

2.2 Extraction of Acoustic Characteristics

The acoustic characteristics mainly refer to the time-domain waveform, spectrum characteristics, and statistical characteristics of the acoustic signal. These characteristics correspond to the characteristic analysis graph of the acoustic signal, such as time-domain

graph, spectrum graph, etc. The time-domain graph and the spectrum graph are two main visual graphs of signal analysis, and the time-domain graph is always used to express the signal visually, while the frequency distribution of the signal on the node is usually reflected in the spectrum graph. However, they both have their own limitations. The frequency information cannot be intuitively presented through the time-domain graph, and spectrum characteristics do not convey how the signal changes over time. For this

reason, the above two methods were both used to respectively analyze the kinematics information and dynamic information of hammering sound, which extracted two brand new indexes from above-mentioned two graphs, amplitude attenuation coefficient (AAC) and high and low frequency ratio (HLFR), as the input parameters of prediction models.

2.2.1 Time-Domain Characteristic

When a geological hammer is used to hit a rock, the energy is released in the form of elastic waves. Thus, the physical and mechanical properties of the rock can be determined by studying the energy and size of the acoustic wave transfer. The time-domain signal can be obtained directly by Python toolbox. Figure 4a, c show that the attenuation velocity of acoustic signals of different rocks vary greatly with time, and the duration of the maximum amplitude is different. The main part of each acoustic signal interval is taken as the research object to find out the law, and the whole

amplitude is transformed into positive value uniformly, thus the change process in the amplitude of the acoustic wave over time is presented completely, as shown in Fig. 4b, d. In order to reflect the attenuation velocity of the acoustic signal well, 0–0.02 s was defined as the large amplitude concentration segment (s_1), and 0–0.04 s was defined as the acoustic signal attenuation research segment (s_2). The area of the two-segment curve and the transverse axis were respectively calculated as S_1 and S_2 . The ratio of S_1 to S_2 was defined as the amplitude attenuation coefficient (AAC). The larger the AAC value, the faster the attenuation velocity of the acoustic signal was.

2.2.2 Spectrum Characterization

Through the analysis of the acoustic spectrum, it was found that the energy was relatively concentrated in the region around 4000 Hz and appeared as sharp resonance peaks, as shown in Fig. 5. The resonance peaks reflect the physical characteristics of the two

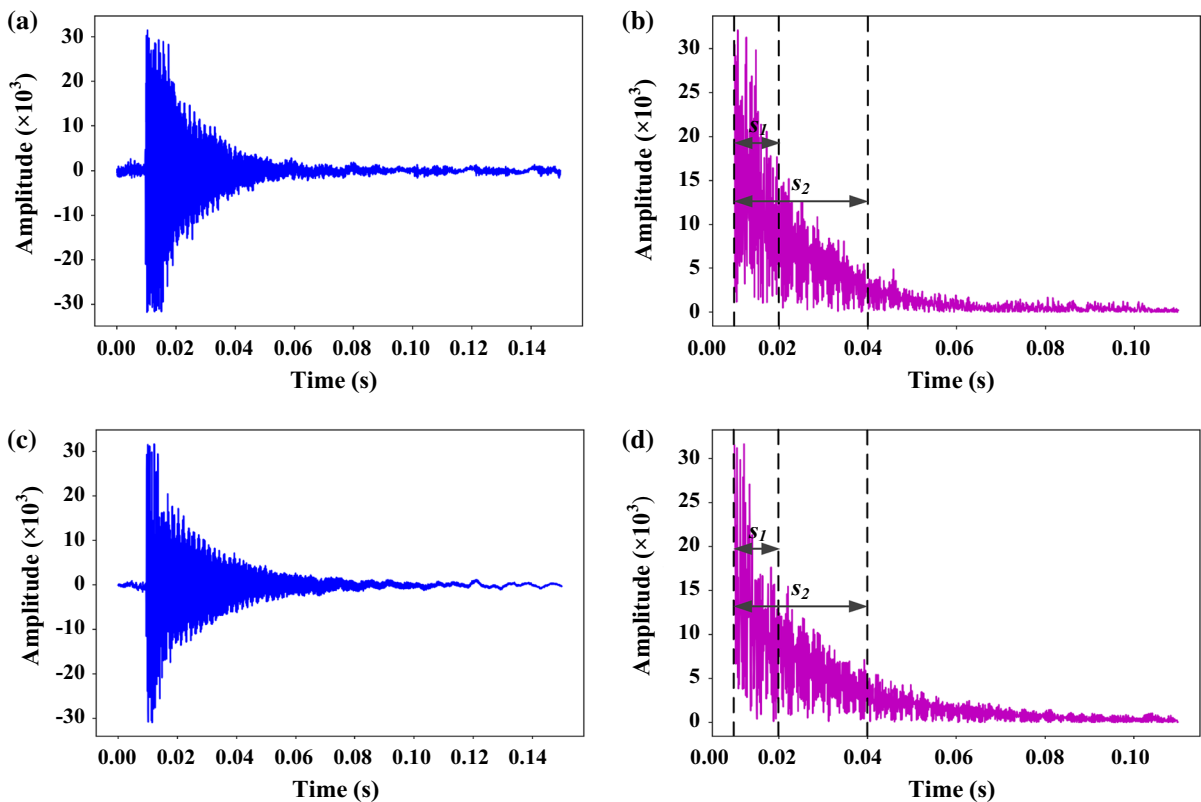


Fig. 4 Time-domain graphs of a single strike on rocks **a** specimen number one and **c** specimen number two; Time-domain transformation graphs of a single strike on rocks **b** specimen number one and **d** specimen number two

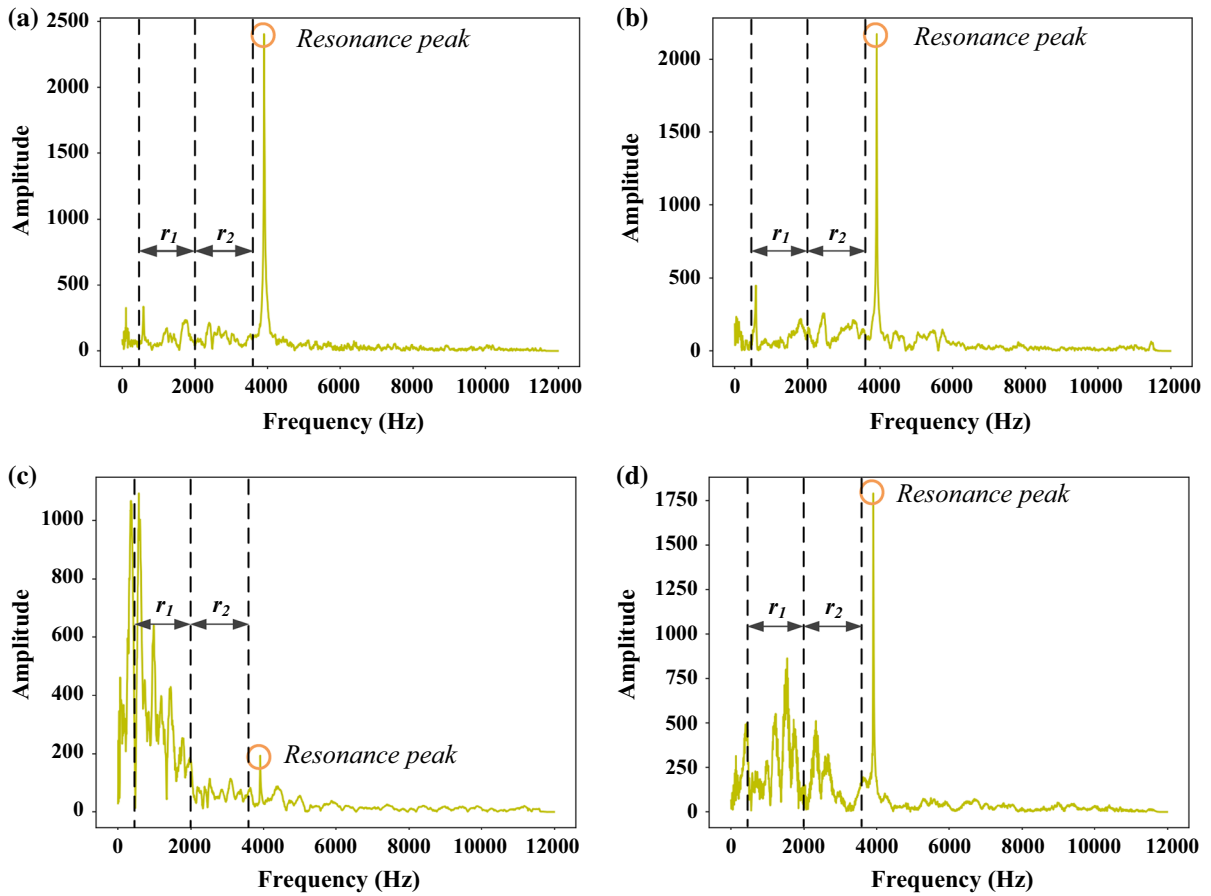


Fig. 5 Spectrum graphs of a single strike on rocks **a** specimen number one, **b** specimen number two, **c** specimen number five, and **d** specimen number seven

channels (resonant cavity) produced by the sounds of both the geological hammer and the rock when the two made contact. This illustrates the natural frequency of the geological hammer is about 4000 Hz. Since this part of the acoustic spectrum contains more energy and does not belong to the elastic wave emitted by the rock itself, only the spectrum at the 500–3800 Hz range can be used as the research area when analyzing the spectrum. Moreover, different hammering sounds were heard when hitting various rocks. Rocks with high strength generally produced a crisp and sharp sound, while rocks with poor properties produced a muddled and dull sound. The spectrum of the single region repetition test of the same rock was very similar, and the spectrum of different rocks was very wide. However, whether the spectrum of a rock with high or low RCS, energy below 2000 Hz accounted for the majority of the spectrum. For comparison,

500–2000 Hz was determined as a low-frequency region (r_1), and 2300–3800 Hz was determined as a high-frequency region (r_2). The area between the low-frequency area (A_1) and the high-frequency area (A_2) between the two-section curve and the horizontal axis were obtained using the integral method, and the ratio of A_2 to A_1 was defined as the high and low frequency ratio (HLFR).

2.3 Signal Label: RCS Measurement by Schmidt Hammer

The Schmidt hammer is widely used in the rebound method, which is a non-destructive method for testing the compressive strength of rock or concrete materials (Brencich et al. 2013). Scholars at home and abroad have studied the measurement of RCS with the Schmidt hammer for more than 50 years (Yaşar and

Erdoğan 2004), therefore the rebound method is well-developed. Moreover, the regression model for elastic modulus of the rock, which is the relationship between the rebound value index and RCS, is well-established (Wang et al. 2017). Thus, for simplifying operation procedures, rapid testing, improving practicality, and decreasing cost while satisfying the requirements of field testing of geological engineering, the rebound method has been adopted to measure RCS indirectly. In the test, we selected nine surface-formed rock specimens, which were carried out in strict accordance with the ISRM suggested methods (Aydin 2008). The final rebound value of each rock was used to mark the corresponding rock hammering signal, as shown in Table 1. Therefore, all the RCS values mentioned in this paper were represented by the rebound value to avoid the error of transformation.

3 Data Modeling and Analysis

The prediction model was established independently based on MLAs to avoid artificial intervention and make more objective predictive analytics (Alpaydin 2014). MLAs also have a comparative advantage in solving complicated prediction problems (Mahdevari et al. 2014; Rodriguez-Galiano et al. 2015; Salazar et al. 2015). Since the acoustic spectrum contained a lot of incomplete and noisy information, it was hard to process it in conventional mathematical statistic methods. Nevertheless, MLAs were able to extract the hidden data pattern or knowledge law from the acoustic spectrum to help to predict RCS accurately. KNN, NB, RF, ANN, and SVM algorithms were chosen to analyze acoustic characteristics and establish regression prediction models.

3.1 Introduction to Algorithms

3.1.1 *K-Nearest Neighbors*

KNN is a predictor of no training parameters and is one of the simplest MLAs (Altman 1992). If any one of the training samples represents a point in the n -dimensional space, all training samples can be stored in the n -dimensional space. When given an unknown sample, KNN is used to search in the n -dimensional space to find the k samples closest to the unknown sample and to predict the value of unknown samples

based on the properties of the k nearest neighbor samples. The proximity between two points $X = (x_1, x_2, \dots, x_n)$ and $Y = (y_1, y_2, \dots, y_n)$ tends to be expressed as Euclidean distance.

3.1.2 *Naive Bayes*

NB is a probabilistic and statistical method based on the Bayes theorem (Farid et al. 2014). It is assumed that the sample belongs to C_i , whose eigenvector is $X = (x_1, x_2, \dots, x_n)$. When the unknown item X is given, the probability of each value is solved using the Bayes theorem, and the largest value of the corresponding probability is considered an estimate of the unknown item. The basic principle of NB can be represented by Bayes formula.

3.1.3 *Random Forest*

RF is an integrated learning method composed of many decision tree models $\{h(X, L_k), k = 1, 2, \dots\}$ (Ho 1998), and $\{L_k\}$ is a random vector of independent distribution and it is used to control the growth of every tree. RF first uses bootstrap sampling to extract k samples from the training set, then establishes a decision tree model for each sample respectively, and finally obtains the sequence $\{h_1(X, L_1), h_2(X, L_2), \dots, h_k(X, L_k)\}$. Under the given independent variable X , each decision tree predicts a value. The final predictive value depends on a simple majority vote for the result of each decision tree. The equation can be expressed as:

$$H(x) = \arg \max_Y \sum_{i=1}^k I(h_i(x, L_i) = C) \quad (1)$$

where $H(x)$ is an RF model, C is the label, and $I(x)$ is an indicator function.

3.1.4 *Artificial Neural Networks*

ANN is a learning method of simulating the identification pattern and logic object of the biological nervous system (Rojas 2013). The adaptive method driven by data makes a few assumptions about the model beforehand, and the main influencing factors include neuron mathematical model, neural network connection, etc. A neural network consists of an input layer, one or more hidden layers, and an output layer.

The signal is first entered through the input layer, then output after the hidden layer is computed. Next, the result of the hidden layer is output by the output layer under the excitation function, and finally the output signal is compared with the desired output. If the error is too large, the error signal is reversed from the output layer to the hidden layer and then propagated to the input layer. The cycle stops until the number of studies is met, or the error can be accepted.

3.1.5 Support Vector Machines

SVM has been widely used to solve regression analysis problems, which are based on the statistical VC dimension theory and the principle of minimum structural risk (Khandelwal and Monjezi 2013). The basic idea of SVM is to find an optimal separation hyperplane through training so that the two kinds of samples can be separated correctly and the error probability is minimized and the separation spacing is maximized.

For the linear problem, the optimal classification plane is transformed into the quadratic programming problem, and the Lagrange multiplier method can be used to solve the constraint optimization problem:

$$\begin{cases} \min f(x) & x \in E^n \\ \text{s.t. } \varphi_i(x) \geq 0 & x \in \{1, 2, \dots, m\} \end{cases} \quad (2)$$

For the non-linear problem, the input variable is transformed into a high dimension space, and the linear separability can be realized by introducing the appropriate kernel function. The best classification plane is:

$$g(x) = \sum_{i=1}^n \alpha_i y_i k(x_i, x) + b \quad (3)$$

where $g(x)$ is a predictor, α_i is a Lagrange multiplier, (x_i, y_i) is a known sample, x is unknown, b is the vertical coordinate of the intersection, and $k(x_i, x)$ is a kernel function.

3.2 Simulation Modeling Experiment

As is known to all, different MLAs are used to solve the same problem, while their forecasting performance and prediction accuracy are not the same. Therefore, it is necessary to select the optimal algorithm for RCS prediction in terms of hammering sound. Based on the

data obtained from tests, five prediction models of KNN, NB, RF, ANN, and SVM were established to analyze acoustic characteristics. The main steps to build a model were outlined below.

3.2.1 Data Preprocessing

Before building a model, all the data needed to be divided into two subsets for training and testing. The general rule was to randomly extract 80% of the available data for training, and the rest were used for testing (Michalski et al. 2013). The training set was used to determine model parameters and establish a prediction model, and the test set was used to evaluate model performance and verify the validity of a model. There were 2014 sound intervals in all, of which 1614 were used as the training set and the other 400 as the test set. According to the result of feature extraction, the output variable was RCS, with the input parameters of AAC and HLFR.

Although inconsistent and wrong data were eliminated before modeling, data conversion was still necessary to ensure the quality of input parameters. With AAC and HLFR mostly ranged from zero to one, data pattern was not obvious, thereby improving prediction errors. In order to highlight the characteristic value and reduce the effect of the program runtime on the convergence speed, AAC and HLFR were amplified together after comparison and verification, which was multiplied by the model coefficient $m = 10$.

3.2.2 Optimization of Model Parameters

The critical parameters of every prediction model were adjusted by K -fold cross validation, thus the corresponding performance was improved. The better execution parameters were selected after performing

Table 2 Better execution parameters of five prediction models

MLAs	Parameters of different models
KNN	$k = 5$
NB	$\alpha = 0.02, \beta = 0.03$
RF	$numTrees = 5, maxDepth = 5$
ANN	$n = 20$
SVM	$C = 10, \gamma = 0.1$

multiple calculations and comparisons, as shown in Table 2. The KNN parameter k represents the number of the nearest neighbors; the NB parameters are the posterior probability α and β ; the RF parameters $numTrees$, $maxDepth$ respectively represent the decision tree number as well as each tree's maximum depth; the ANN parameter is the hidden layer number n ; the SVM parameters are the penalty factor C and the width of Gaussian radial basis kernel function (RBF) parameter γ .

3.2.3 Evaluation of Model Reliability

After training and testing the five models, the predicted values were compared with 45 measured values selected from 400 test samples for the sake of evaluating the reliability of five prediction models. As shown in Fig. 6, the scattered points represent the measured values. The errors between the predicted values and measured values are presented in Fig. 7, which can directly reflect the deviation degree of the predicted values from measured values. At the same time, the accuracy and stability of each model were evaluated by four statistic indexes (or performance measures) to verify whether the model could realize quantitative prediction, such as coefficient of determination (R^2), mean absolute error (MAE), root mean square error (RMSE), and mean absolute percent error (MAPE). Theoretically, the prediction model works best when R^2 equals one and MAE, RMSE, and MAPE equal zero. Table 3 summarizes the performance measures of the five models for the training dataset.

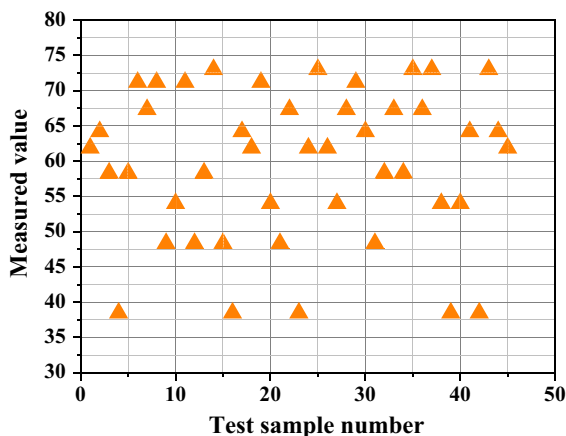


Fig. 6 Distribution of 45 measured rebound values selected from 400 test samples

The results showed ANN and SVM performed better than KNN, NB, and RF. Table 4 summarizes the performance measures of the five models for the test samples. The results obviously indicated that ANN and SVM had superior performance and that their performance levels were very close. It can be seen from Fig. 7 that the NB model had the greatest deviation from the measured value, as well as the largest degree of dispersion. The overall prediction results of the KNN and RF model were better, but the RCS errors of individual rock specimens were greater. The SVM and ANN model predicted the highest accuracy of RCS. Therefore, SVM and ANN were better for widespread application in the prediction of RCS based on acoustic characteristics.

3.3 Characteristic Mechanism of Acoustic Spectrum

3.3.1 Correlation Analysis

With the help of the dual-variable Pearson correlation analysis function of SPSS, a parametric correlation analysis of acoustic characteristics (AAC and HLF) and RCS were conducted respectively with the results as shown in Table 5. The Pearson correlation analysis showed that confidence levels of the two characteristics were both more than 0.9, which signifies that the two characteristics were highly correlated with RCS. In order to further understand the change trend between acoustic characteristics and RCS, Fig. 8a, b showed the scatter plots between two characteristics and RCS respectively. According to the curve fitting of the scatter points, it was found that the RCS was roughly linear with the two characteristics, and the R^2 of each was more than 0.9.

3.3.2 Mechanism Study

Based on the study of the mechanical characteristics of rock by analyzing the acoustic signal spectrum, the relationship between acoustic characteristics (AAC and HLF) and RCS was determined by comparing the predicted value with the measured value, correlation analysis, and curve fitting, etc. RCS was closely related to its mineral composition, inter-granular connection, structural characteristics, weathering and fragmentation degree, particle size and shape. In this work, the intrinsic mechanism of the correlation

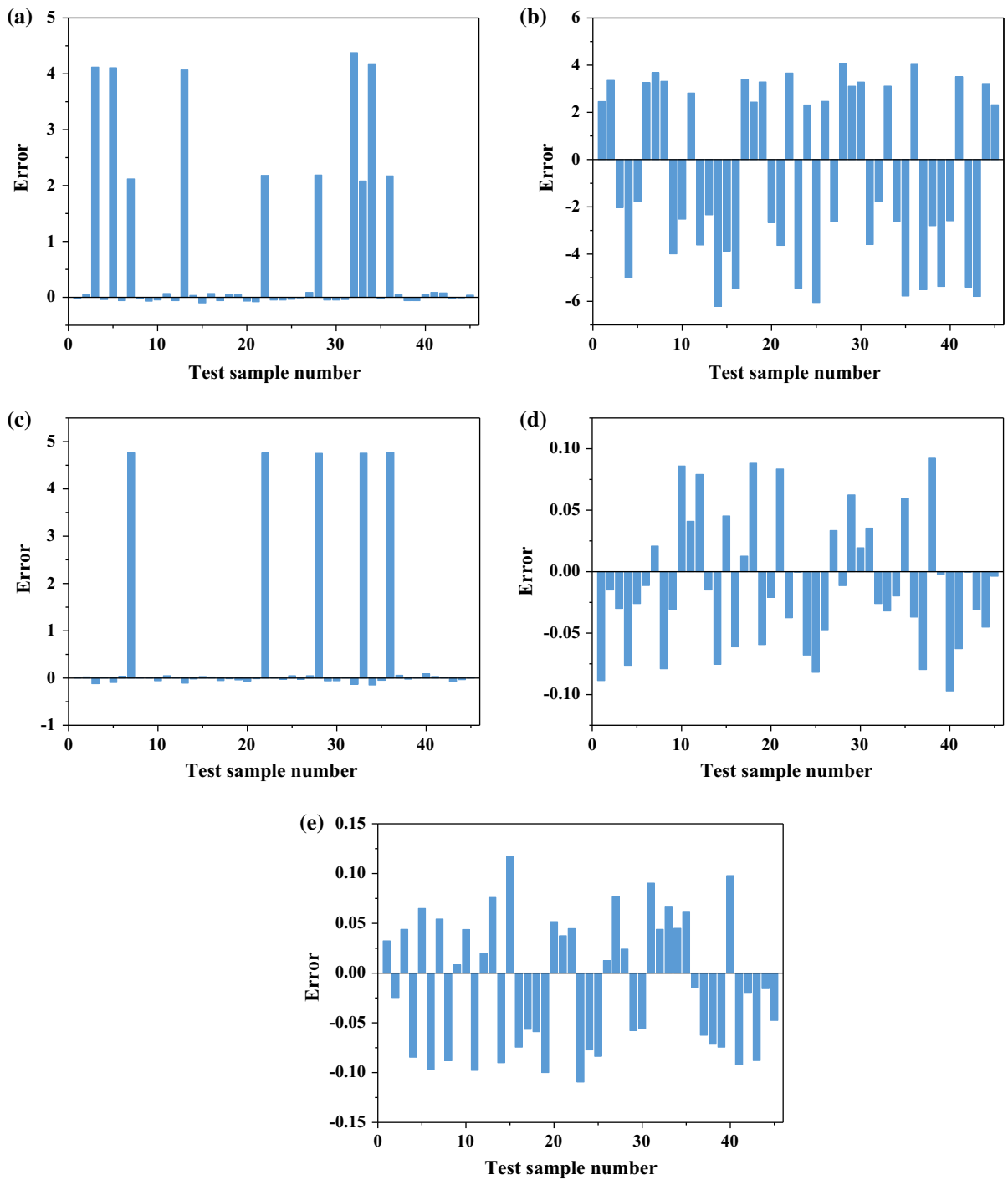


Fig. 7 The errors between measured values and predicted values of five models **a** KNN, **b** NB, **c** RF, **d** ANN, and **e** SVM

between RCS and acoustic characteristics was further studied, and the attenuation characteristics and

frequency change of hammering sound were transformed from the natural characteristics of the rock itself.

Table 3 Performance measures for training set

MLAs	Sample size of training set	Four statistic indexes			
		R ²	MAE	RMSE	MAPE
KNN	1614	0.9832	0.1332	0.5973	0.2237
NB		0.8802	3.6703	3.8422	6.4912
RF		0.9784	0.4107	1.1028	0.6426
ANN		0.9873	0.1351	0.2740	0.2011
SVM		0.9913	0.0676	0.0817	0.1125

Table 4 Performance measures for test set

MLAs	Sample size of test set	Four statistic indexes			
		R ²	MAE	RMSE	MAPE
KNN	400	0.9826	0.1375	0.5956	0.2250
NB		0.8768	3.7084	3.9403	6.6941
RF		0.9731	0.6730	1.7627	1.0464
ANN		0.9874	0.1263	0.2752	0.2033
SVM		0.9906	0.0916	0.1009	0.1248

Table 5 Results of correlation analysis between acoustic characteristics and RCS

Acoustic characteristics	Total number of samples	Pearson correlation coefficient <i>r</i>	Degrees of correlation
AAC	2014	− 0.9072	High-negative correlation
HLFR	2014	0.9209	High-positive correlation

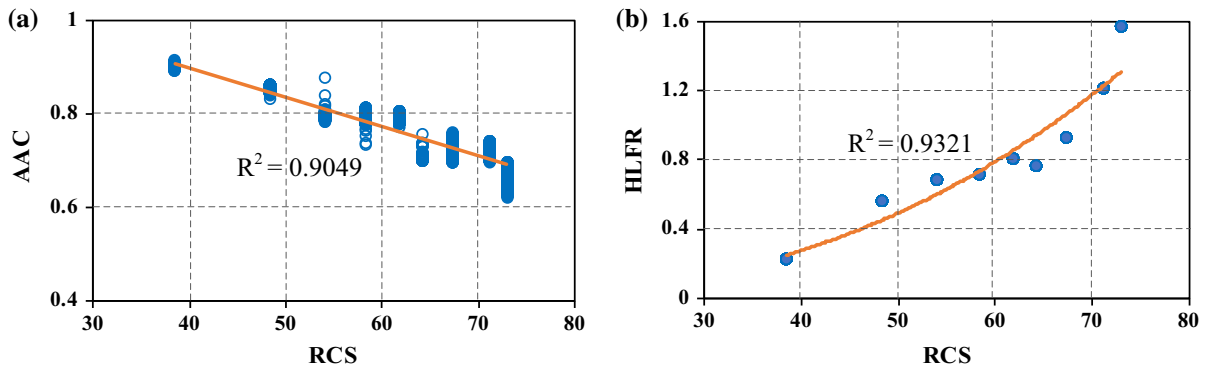


Fig. 8 Relationship diagrams **a** relationship between AAC and RCS, and **b** relationship between HLFR and RCS

It can be seen from Fig. 4 that the initial amplitude of each hammering signal was around 30000, and the amplitude decreased gradually to zero after some time. The signal attenuation was led by energy dissipation. Thus, we tried to figure out the reason for energy dissipation when the initial energy of the acoustic signal was approximately the same. The sound signal

spread to the surrounding when hammering at the surface of the rock. The complete signal was composed of two parts of sounds generated by hitting the rock: one that traveled through the air and the other that traveled into the rock medium and reflected from the medium surface layer. The former is roughly the same, while the latter is easily influenced by the

Table 6 The correlation of RCS rating with AAC and HLFR based on Chinese standard

Degrees of solidity	Hard rock	Fairly hard rock	Fairly soft rock	Soft rock (including the extremely soft rock)
RCS	> 48.91	33.23–48.91	17.55–33.23	< 17.55
AAC	< 0.84	0.84–0.93	0.93–1.00	> 1.00
HLFR	> 0.45	0.22–0.45	0.10–0.22	< 0.10

characteristics of the rock itself. The weaker rock was susceptible to chemical weathering and easily decomposed into secondary hydrophilic minerals. This caused the inter-particle connection state to transform into a water-glu connection, which formed a discontinuous spatial structure of the two different dielectric phases of the mineral and air (or water). The acoustic signal passed through the mineral-air (or water) medium once, while energy loss occurred once. The more the dielectric surface exists, the more energy was lost, and the faster the signal decayed. Most of the stronger rocks were crystalline and had higher density. The internal continuous grain composition could be regarded as a single dielectric body, and the signal energy decayed slowly when passing through the medium.

With regard to the frequency change of acoustic signals, the developed method transformed them into the problem of filter effect of different mediums. As shown in Fig. 5, the low-frequency components were greater than the high-frequency components in the signal of the weaker rock, whereas the opposite was true for the stronger rock. Any medium has an absorption effect on the acoustic waves, and the medium has a frequency selective absorption and scattering effect on the acoustic waves. The characteristics of the acoustic wave propagation medium were different, as well as the absorption and scattering of the waves. Because of the severe physical weathering and more tectonic fissures, the weaker rock had a weaker inter-granular connection, which led to more pores in the grains, looser structure, and more porous structures similar to honeycomb. Thus, the absorption of the acoustic wave was enhanced and the penetration ability of the wave was greatly weakened. It was shown that the loss of the high-frequency part of the signal was substantial, which caused the HLFR to become smaller. Because the integrity of the stronger rock was better, the acoustic absorption was smaller.

Therefore, the frequency components were richer and high-frequency components formed the subject of the signal, which caused the HLFR to be larger.

3.3.3 Discussion: Practical Inquiry

We put forward a new approach to measure RCS in field operation by hammering sound after studying the relationship between RCS and acoustic characteristics in detail. Compared with the traditional indirect testing method, this method can be applied to more qualities of rock specimens and suitable for field measurement. It is possible to adopt it for rock mass classification to make up for the shortcomings of the existing methods and play a greater role. Thus, the correlation of RCS rating with AAC and HLFR can be used to distinguish material properties of rock masses. The rock mass quality was established based on Chinese standard (China 1995) of engineering classification of rock masses. The brand new acoustic characteristic indexes, AAC and HLFR, were added to the classification standard to refine the corresponding specification, as shown in Table 6. The better classification will be accepted by using comprehensive indexes to quantify rock mass quality.

4 Conclusions

A new and non-destructive testing method to determine RCS based on MLAs and spectrum analysis of geological hammer was proposed in the paper. The hammering sound samples were successively pre-processed by signal enhancement algorithm and double-threshold method to eliminate noise. Our work established five prediction models of RCS in accordance with acoustic characteristics of AAC and HLFR. The above-mentioned five MLAs were used for performance evaluation and mechanism analysis,

and we ultimately obtained the following conclusions according to the evaluation result and the mechanism explanation: (1) The prediction models of RCS based on SVM and ANN were better than the other three models, and the predicted value was well close to the measured value. And, the SVM model was slightly superior in the prediction accuracy evaluation index. (2) Two brand new indexes of acoustic signal were put forward to simplify the prediction problem, i.e., AAC could reflect the attenuation velocity of the acoustic signal well, while HLFER can represent the energy of the sound signal. The nature of acoustic signal of geological hammer would be reflected with a mixture of both, thereby grading the rock mass quality. (3) The combination of multitaper estimation and spectral subtraction and the improved double-threshold algorithm were adopted for signal preprocessing, thus improving the accuracy of RCS prediction. (4) By analyzing the relationship between RCS and acoustic characteristics, it can be concluded that the greater the RCS, the smaller the AAC and the more slowly the acoustic signal decayed, in the meantime, the greater the HLFER and the high-frequency components were richer, and vice versa. (5) The new method will deserve extensive application in geological surveys and construction acceptance to predict RCS conveniently and accurately based on spectrum analysis of geological hammer.

Note that the rebound value was used to represent RCS for the convenience of rock strength acquisition. However, the accuracy of rebound value is generally low, which is bound to affect the precision of RCS prediction. The high-precision test techniques such as ultrasonic-rebound combined method and uniaxial compression test will be adopted to measure RCS in future research, thus reducing the interference of measurement errors.

Acknowledgements This research was supported by the National Natural Science Foundation for Excellent Young Scientists of China (Grant No. 51622904), the Tianjin Science Foundation for Distinguished Young Scientists of China (Grant No. 17JCJQC44000) and the National Natural Science Foundation of China (Grant No. 51621092).

References

- Alpaydin E (2014) Introduction to machine learning. MIT Press, Cambridge
- Altman NS (1992) An introduction to kernel and nearest-neighbor nonparametric regression. *Am Stat* 46(3):175–185
- Aydin A (2008) ISRM suggested method for determination of the Schmidt hammer rebound hardness: revised version. In: Ulusay R (ed) *The ISRM suggested methods for rock characterization, testing and monitoring: 2007–2014*. Springer, Heidelberg, pp 25–33
- Berouti M, Schwartz R, Makhoul J (1979) Enhancement of speech corrupted by acoustic noise. In: *Acoustics, speech, and signal processing, IEEE international conference on ICASSP*, pp 208–211
- Boashash B (2015) *Time-frequency signal analysis and processing: a comprehensive reference*. Academic Press, New York
- Brencich A, Cassini G, Pera D, Riotto G (2013) Calibration and reliability of the rebound (Schmidt) hammer test. *Civil Eng Archit* 1(3):66–78
- BS5930 (1981) *Code of practice for site investigations*. British Standards Institution, London
- China MWR (1995) *Standard for engineering classification of rock masses (GB50218-94)*. China Planning Press, Beijing
- Farid DM, Zhang L, Rahman CM, Hossain MA, Strachan R (2014) Hybrid decision tree and naive Bayes classifiers for multi-class classification tasks. *Expert Syst Appl* 41(4):1937–1946
- Fattahi H (2017) Applying soft computing methods to predict the uniaxial compressive strength of rocks from Schmidt hammer rebound values. *Comput Geosci* 21(4):665–681
- Fattahi H, Karimpouli S (2016) Prediction of porosity and water saturation using pre-stack seismic attributes: a comparison of Bayesian inversion and computational intelligence methods. *Comput Geosci* 20(5):1075–1094
- Hack R, Huisman M (2002) Estimating the intact rock strength of a rock mass by simple means. In: *Proceedings of 9th congress of the International Association for Engineering Geology and the Environment*, Durban, pp 16–20
- Hencher SR, Richards LR (2015) Assessing the shear strength of rock discontinuities at laboratory and field scales. *Rock Mech Rock Eng* 48(3):883–905
- Ho TK (1998) The random subspace method for constructing decision forests. *IEEE Trans Pattern Anal Mach Intell* 20(8):832–844
- Jordan MI, Mitchell TM (2015) Machine learning: trends, perspectives, and prospects. *Science* 349(6245):255–260
- Karakus M, Tutmez B (2006) Fuzzy and multiple regression modelling for evaluation of intact rock strength based on point load, Schmidt hammer and sonic velocity. *Rock Mech Rock Eng* 39(1):45–57
- Karaman K, Kesimal A (2015) A comparative study of Schmidt hammer test methods for estimating the uniaxial compressive strength of rocks. *Bull Eng Geol Environ* 74(2):507–520
- Khandelwal M, Monjezi M (2013) Prediction of backbreak in open-pit blasting operations using the machine learning method. *Rock Mech Rock Eng* 46(2):389–396
- Kido KI (2015) *Digital Fourier analysis: fundamentals*. Undergraduate lecture notes in physics. Springer, New York

- Lee C, Hyun D, Choi E, Go J (2003) Optimizing feature extraction for speech recognition. *IEEE Trans Audio Speech Process* 11(1):80–87
- Li Q, Zheng J, Tsai A, Zhou Q (2002) Robust endpoint detection and energy normalization for real-time speech and speaker recognition. *IEEE Trans Audio Speech Process* 10(3):146–157
- Li F, Wang JA, Brigham JC (2014) Inverse calculation of in situ stress in rock mass using the surrogate-model accelerated random search algorithm. *Comput Geotech* 61:24–32
- Mahdevari S, Shahriar K, Yagiz S, Shirazi MA (2014) A support vector regression model for predicting tunnel boring machine penetration rates. *Int J Rock Mech Min Sci* 72:214–229
- Marinos P, Hoek E (2001) Estimating the geotechnical properties of heterogeneous rock masses such as flysch. *Bull Eng Geol Environ* 60(2):85–92
- Michalski RS, Carbonell JG, Mitchell TM (2013) *Machine learning: an artificial intelligence approach*. Springer, Berlin
- Mohamad ET, Armaghani DJ, Momeni E, Abad SVANK (2015) Prediction of the unconfined compressive strength of soft rocks: a PSO-based ANN approach. *Bull Eng Geol Environ* 74(3):745–757
- Momeni E, Armaghani DJ, Hajihassani M, Amin MFM (2015) Prediction of uniaxial compressive strength of rock samples using hybrid particle swarm optimization-based artificial neural networks. *Measurement* 60:50–63
- Rodriguez-Galiano V, Sanchez-Castillo M, Chica-Olmo M, Chica-Rivas M (2015) Machine learning predictive models for mineral prospectivity: an evaluation of neural networks, random forest, regression trees and support vector machines. *Ore Geol Rev* 71:804–818
- Rojas R (2013) *Neural networks: a systematic introduction*. Springer, Berlin
- Salazar F, Toledo MA, Oñate E, Morán R (2015) An empirical comparison of machine learning techniques for dam behaviour modelling. *Struct Saf* 56:9–17
- Thomson DJ (1982) Spectrum estimation and harmonic analysis. *Proc IEEE* 70(9):1055–1096
- Ulusay R (2014) *The ISRM suggested methods for rock characterization, testing and monitoring: 2007–2014*. Springer, Heidelberg
- Valera M, Guo Z, Kelly P, Matz S, Cantu A, Percus AG, Hyman JD, Srinivasan G, Viswanathan HS (2018) Machine learning for graph-based representations of three-dimensional discrete fracture networks. *Comput Geosci*. <https://doi.org/10.1007/s10596-018-9720-1>
- Wang H, Lin H, Cao P (2017) Correlation of UCS rating with Schmidt hammer surface hardness for rock mass classification. *Rock Mech Rock Eng* 50(1):195–203
- Yaşar E, Erdoğan Y (2004) Estimation of rock physico-mechanical properties using hardness methods. *Eng Geol* 71(3):281–288